

The Dubna-Mainz-Taipei Dynamical Model for πN Scattering and π Electromagnetic Production

Shin Nan YANG¹

¹*Department of Physics and Center for Theoretical Sciences, Taipei 10716, Taiwan*

E-mail: snyang@phys.ntu.edu.tw

(Received October 5, 2015)

Some of the featured results of the Dubna-Mainz-Taipei (DMT) dynamical model for πN scattering and π^0 electromagnetic production are summarized. These include results for threshold π^0 production, deformation of $\Delta(1232)$, and the extracted properties of higher resonances below 2 GeV. The excellent agreement of DMT model's predictions with threshold π^0 production data, including the recent precision measurements from MAMI establishes results of DMT model as a benchmark for experimentalists and theorists in dealing with threshold pion production.

KEYWORDS: πN scattering, electromagnetic production of pions, meson-exchange model

1. Introduction

Dynamical approach to meson electromagnetic production has been widely employed to analyze and interpret experimental data since it was proposed in [1, 2]. There are now many dynamical models constructed. Currently, the most sophisticated dynamical model ever constructed is the Argonne-Osaka dynamical coupled-channel model [3], as presented by Kamano in this conference [4]. It includes eight channels and 487 parameters.

In this talk, I will summarize the results obtained with Dubna-Mainz-Taipei (DMT) meson-exchange dynamical model for πN scattering and electromagnetic (EM) production of pion. It was prompted by the following motivations. First, to construct a meson-exchange model for πN scattering and EM production of pion in order to achieve a unified description for both reactions over a wide range of energies, i.e., from threshold to c.m. energies $W \leq 2$ GeV. This is important since the extractions of the resonances properties like mass, width, and form factors would be reliable only from a consistent framework. Consistent extractions would help to minimize model dependence such that comparison with LQCD results would be meaningful. Next is that the comparison of threshold results with ChPT predictions would offer a glimpse of the working of chiral symmetry. Lastly, since all dynamical models always assume a picture of bare quark core dressed by pion cloud, the success of the results could help to understand the underlining dynamics of the structure of nucleon resonances.

Among all the dynamical models available on the market, DMT model distinguishes itself in that it can describe all the data well from threshold, including the recent very precise ones from MAMI and Jlab, up to $W \leq 2$ GeV, even though it includes only two channels. It was constructed over a period of about 20 years. It started in 1985 when the dynamical approach was proposed in [2], where it was shown that with the use of separable πN potential, reasonable description of the S- and P-waves $\gamma\pi$ multipoles can be achieved within the dynamical approach. When the experiments [5] from Saclay and MAMI reported the violation of low-energy theorem for the π^0 threshold production, we demonstrated in [6] that the violation could arise from the πN final-state interaction (FSI), again with the use of separable πN interaction. This prompted us, together with Harry Lee, to undertake the task of constructing a realistic meson-exchange (MEX) πN potential. The use a MEX πN model did bring

the threshold values of $E_{0^+}(p\pi^0)$ quite close [7] to the data even though the energy dependence is not well reproduced. With the completion of Taipei-Argonne MEX πN model [8, 9], groups from Dubna and Mainz joined to imbed the Taipei-Argonne MEX πN model within the dynamical approach for πN and $\gamma\pi$ reactions and extend the model to higher energies as well as electroproduction to become the DMT model [10–12].

In the followings, we will first present the basic formulation of the DMT model before summarizing the main results of the model. It will be seen that DMT model gives excellent description of most of the available threshold data, including the recent ones from MAMI. Regarding the resonances properties, we will cover deformation of the $\Delta(1232)$ and the extracted masses and widths of resonances up to 2 GeV and compare them with PDG values.

2. Formulation of the DMT Dynamical Model

2.1 πN scattering

For the πN scattering, we start with the Bethe-Salpeter (BS) equation,

$$T_{\pi N} = B_{\pi N} + B_{\pi N} G_0 T_{\pi N}, \quad (1)$$

where $B_{\pi N}$ is the sum of all irreducible two-particle Feynman amplitudes and G_0 the free relativistic πN propagator. The four-dimensional BS equation can be reduced to a three-dimensional one by first recasting it into following two equations,

$$T_{\pi N} = \hat{B}_{\pi N} + \hat{B}_{\pi N} \hat{G}_0 T_{\pi N}, \quad (2)$$

$$\hat{B}_{\pi N} = B_{\pi N} + B_{\pi N} (G_0 - \hat{G}_0) \hat{B}_{\pi N}, \quad (3)$$

so that Eq. (2) would become three-dimensional with an appropriate choice of propagator $\hat{G}_0(k; P)$. It is important to choose \hat{G}_0 such that two-body unitarity is maintained by reproducing the πN elastic cut. There is a wide range of possible propagators that satisfy this requirement. Since chiral symmetry plays an essential role in strong interaction, we employ the Cooper-Jennings propagator [13] as it satisfies both the soft pion theorems and unitarity. Furthermore, we approximate $\hat{B}_{\pi N}$ by the tree diagrams of a chiral invariant Lagrangian consisting of π , N , σ , ρ , and $\Delta(1232)$ fields with pseudovector couplings, if interest is restricted from threshold to first resonance region.

For higher energies, we have to include the ηN channel as it is well-known that it couples strongly with the two lowest S_{11} resonances. In addition, we introduce more resonances as dictated by the data. They are all bare and get dressed by the meson cloud as in the case of $\Delta(1232)$. The effects of the $\pi\pi N$ channel are accounted for with introduction of a phenomenological width to the bare resonances. The details are given in [14–17].

The parameters in the model like coupling constants, cut-off in the form factors, and bare masses of the resonances are then varied to obtain best fit to the phase shifts and inelasticities.

2.2 $\gamma\pi$ reactions

The dynamical approach to the EM production of pions starts with the following Lippman-Schwinger equation,

$$t_{\gamma\pi}(E) = v_{\gamma\pi} + v_{\gamma\pi} g_0(E) t_{\pi N}(E), \quad (4)$$

where $v_{\gamma\pi}$ is the $\gamma\pi$ transition potential, g_0 and $t_{\pi N}$ are the πN free propagator and t -matrix, respectively, and E is the total energy in the c.m. frame. $t_{\pi N}$ is related to T defined in Eq. (1) by some kinematical factor. $v_{\gamma\pi}$ are derived from an effective Lagrangian obtained from gauging the chiral invariant Lagrangian used for the πN scattering. It contains Born terms as well as ρ - and

ω -exchange in the t -channel [18]. For electroproduction, gauge invariance is restored by the substitution, $J_\mu \rightarrow J_\mu - k_\mu \frac{k \cdot J}{k^2}$, where J_μ is the electromagnetic current corresponding to the background contribution of $v_{\gamma\pi}^B$.

For the physical multipoles in channel $\alpha = \{l, j\}$, Eq. (4) gives [2]

$$t_{\gamma\pi}^\alpha(q_E, k) = \exp(i\delta^\alpha) \cos \delta^\alpha \left[v_{\gamma\pi}^\alpha(q_E, k) + P \int_0^\infty dq' \frac{R_{\pi N}^\alpha(q_E, q') v_{\gamma\pi}^\alpha(q', k)}{E(q_E) - E(q')} \right], \quad (5)$$

where δ^α and R^α are the πN phase shift and reaction matrix, in channel α , respectively, q_E is the pion on-shell momentum and $k = |\mathbf{k}|$ the photon momentum. Note that the second term on the r.h.s. of the principal integral term in Eq. (5), depends on the off-energy-shell behaviors of both $R_{\pi N}^\alpha$ and $v_{\gamma\pi}^\alpha$. To maintain gauge invariance for the off-energy-shell matrix elements of $v_{\gamma\pi}^\alpha$ is a nontrivial task and different groups have followed different recipes. The prescription we used are expounded in [16].

3. Results and Discussions

In this section we summarize some of the featured results of DMT model. This includes threshold π^0 production, $\Delta(1232)$ deformation, and the extracted properties of the higher resonances.

3.1 Threshold π^0 production

The discrepancy between experiments [5] and the prediction of low-energy theorem based on current algebra and PCAC, for the π^0 threshold production came as a big surprise. First it was suggested [6] that the discrepancy could arise from the πN final-state interaction (FSI). Soon it was recognized the EM threshold π^0 production provides an excellent arena to study spontaneous as well as explicit chiral symmetry breaking with latter arising from the non-vanishing small masses of u and d quarks. This has spurred intensive theoretical and experimental efforts which persist until today.

On the theoretical side, two different approaches have been undertaken, namely, dynamical model and chiral perturbation theory (ChPT) [19]. In the followings, results from DMT model, the most successful dynamical model for the threshold pion production, are compared with predictions of relativistic chiral perturbation theory (RChPT) [20, 21], heavy baryon chiral perturbation theory (HBChPT) [22], and the latest measurements from MAMI.

We show in Fig. 1, the real and imaginary parts of the $E_{0+}(p\pi^0)$ near threshold. The blue dashed curve denotes the result obtained without FSI in DMT. The black solid and red dot-dot-dashed lines correspond to the predictions of the full DMT model and the HBChPT, respectively. The data are from [5]. It is seen that both DMT model and HBChPT can describe the data well. The green dot-dashed and purple dotted curves are the results obtained with one-loop and two-loop corrections included within DMT model, namely, $t_{\gamma\pi}(E)$ is approximated with $v_{\gamma\pi} + v_{\gamma\pi}g_0(E)v_{\pi N}(E)$ and $v_{\gamma\pi} + v_{\gamma\pi}g_0(E)v_{\pi N}(E) + v_{\gamma\pi}g_0(E)v_{\pi N}(E)g_0(E)v_{\pi N}(E)$, respectively. One sees that

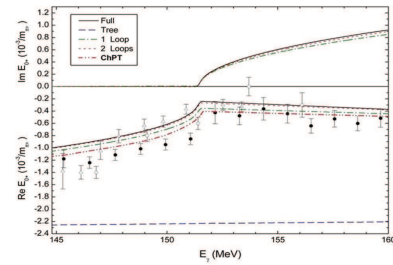


Fig. 1. Comparison of predictions of DMT model, HBChPT with data for $E_{0+}(p\pi^0)$ near threshold. See text for notations.

the two-loop corrections are small and ChPT calculations is justified to stop within the one-loop scheme.

Fig. 2 shows the coincidence cross sections σ_0 , σ_{TT} , and σ_{LT} in $\mu\text{b}/\text{sr}$ and beam asymmetry A_{LT} in % measured at MAMI [23] in π^0 electroproduction at constant $Q^2 = 0.05 \text{ GeV}^2$, $\Theta_\pi = 90^\circ$, $\Phi_\pi = 90^\circ$, and $\epsilon = 0.93$ as a function of ΔW above threshold. The red solid lines show RChPT calculations at $O(q^4)$ and the black dotted lines are the heavy-baryon ChPT calculations of [22]. The green dashed curves are obtained from DMT model. It is seen that the data are in disagreement with predictions of HBChPT, while in good agreement with DMT model and RChPT predictions with DMT doing somewhat a better job. In Fig. 3, the polarised differential cross sections σ_T of threshold π^0 photoproduction with transverse polarized protons measured at MAMI for photon energies at 168.5 and 183.7 MeV, respectively, are depicted [24]. Data points represent Crystal Ball/TAPS results with statistical uncertainties only. Solid lines are predictions of the DMT model, while dashed and dashed-dotted lines show three-parameter Legendre fits to the experimental data and the cross-check analysis, respectively. Again DMT model describes these data very well.

The success of DMT model in describing EM π^0 production near threshold can be understood as follows. In Eq. (4), it is seen that the $t_{\gamma\pi}$ depends only on $v_{\gamma\pi}$ and $t_{\pi N}$. In the threshold region, only background mechanisms contribute, namely, $v_{\gamma\pi}$ and $t_{\pi N}$ would be given by $v_{\gamma\pi}^B$ and $t_{\pi N}^B$, respectively, where superscript B refers to background mechanism. Since $v_{\gamma\pi}^B$ and $v_{\pi N}^B$, which drives $t_{\pi N}^B$, are both derived from tree diagrams of chiral invariant effective Lagrangian, and we use Cooper-Jennings' propagator which satisfies soft-pion theorem to generate $t_{\pi N}^B$, it is not surprising that the resulting $t_{\gamma\pi}^B$ would preserve many of the consequences of chiral symmetry.

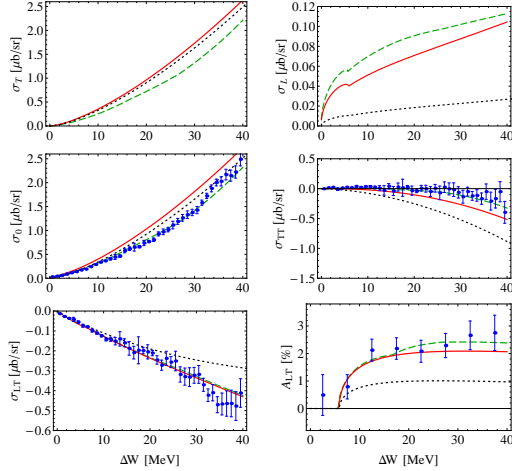


Fig. 2. σ_0 , σ_{TT} , and σ_{LT} and A_{LT} at $Q^2 = 0.05 \text{ GeV}^2$, $\Theta_\pi = 90^\circ$, $\Phi_\pi = 90^\circ$, and $\epsilon = 0.93$ vs. ΔW . See text for notations.

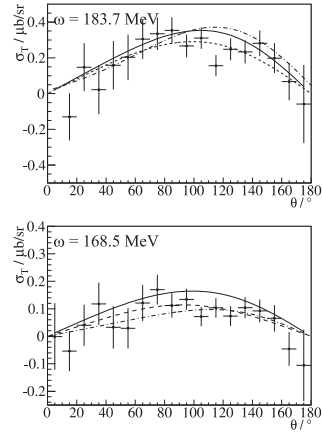


Fig. 3. σ_T . Data points represent Crystal Ball/TAPS results with statistical uncertainties only. See text for notations.

3.2 (3,3) Multipoles M_{1+} , E_{1+} and the Deformation of $\Delta(1232)$

In the begining, the dynamical approach was proposed for the first resonance region [1,2] in order to unitarize the $\gamma\pi$ multipoles to satisfy the Fermi-Watson theorem dynamically. In the (3,3) channel where Δ excitation plays an important role, the transition potential $v_{\gamma\pi}$ consists of two terms

$$v_{\gamma\pi}(E) = v_{\gamma\pi}^B + v_{\gamma\pi}^\Delta(E), \quad (6)$$

where $v_{\gamma\pi}^B$ is the background transition potential which, as discussed earlier, includes Born terms and vector mesons exchange contributions. The second term of Eq. (6) corresponds to the contribution

of bare Δ , namely, $\gamma^*N \rightarrow \Delta \rightarrow \pi N$. The vertex $\gamma^*N \rightarrow \Delta$ would introduce three more parameters corresponding to $M1$, $E2$, and $C2$ excitations.

We proceed by decomposing Eq. (4) in the following way,

$$t_{\gamma\pi} = t_{\gamma\pi}^B + t_{\gamma\pi}^\Delta, \quad (7)$$

where

$$t_{\gamma\pi}^B(E) = v_{\gamma\pi}^B + v_{\gamma\pi}^B g_0(E) t_{\pi N}(E), \quad (8)$$

$$t_{\gamma\pi}^\Delta(E) = v_{\gamma\pi}^\Delta + v_{\gamma\pi}^\Delta g_0(E) t_{\pi N}(E). \quad (9)$$

The advantage of such a decomposition (7) is that both $t_{\gamma\pi}^B$ and $t_{\gamma\pi}^\Delta$ would satisfy the Fermi-Watson theorem as can be inferred from Eq. (5). $t_{\gamma\pi}^\Delta$ would contain all the processes which start with the electromagnetic excitation of the bare Δ . It provides a prescription to extract information concerning bare Δ excitation.

With $t_{\pi N}$ obtained as prescribed in Sec. 2.1, $t_{\gamma\pi}^B$ can be calculated straightforwardly. For real

photon, $t_{\gamma\pi}^\Delta$ depends on the $M1$ and $E2$ excitation strength of $\gamma N \rightarrow \Delta$. By combining the contributions of $t_{\gamma\pi}^B$ and $t_{\gamma\pi}^\Delta$ with the excitation strength as free parameters, results of our best fit to the real and imaginary parts of the $M_{1+}^{(3/2)}$ and $E_{1+}^{(3/2)}$ multipoles obtained in the analyses of Mainz [25] and VPI group [26] are shown in Fig. 4. The dashed (dotted) curves are the results obtained within the DMT model for $t_{\gamma\pi}^B$ including (excluding) the principal value integral contribution in Eq. 5. The solid curves are the full DMT results including also the bare Δ excitation. For the E_{1+} multipole, the dashed and solid curves practically coincide due to the small value of the bare Δ contribution. The open and solid circles are the results from the Mainz and VPI analyses, respectively. In other words, The purple and yellow regions represented the the contributions from bare Δ excitation and the off-energy-shell πN rescatterings associated with pion cloud.

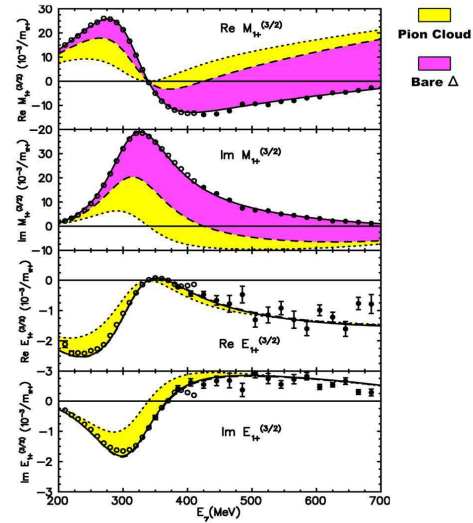


Fig. 4. Our results for $M_{1+}^{(3/2)}$ and $E_{1+}^{(3/2)}$ multipoles. See text for notations. Figure from [10].

At low four-momentum transfer squared Q^2 , the interest in the EM excitation of Δ lies in the observation of a D -state in Δ [27–29]. It would indicate that Δ is deformed and the photon can excite a nucleon via $E2$ and $C2$ transitions. In a symmetric $SU(6)$ quark model, the electromagnetic excitation of Δ could proceed only via $M1$ transition. In pion electroproduction, $E2$ and $C2$ excitations would give rise to nonvanishing $E_{1+}^{(3/2)}$ and $S_{1+}^{(3/2)}$ multipole amplitudes. Currently, summary of experiments give, near $Q^2 = 0$ and at $W = 1232$ MeV, $R_{EM} = E_{1+}^{(3/2)}/M_{1+}^{(3/2)} = -(2.5 \pm 0.5)\%$ [32], whereas we obtained a value of 0.24%, a clear indication of Δ deformation.

Our results shown in Fig. 4 offer an interesting dynamical picture for the $\Delta(1232)$ deformation. Namely, bare Δ contribution to E_{1+} , as would be denoted in red, nearly vanishes. It implies that the bare Δ is mostly spherical as would be in a symmetric $SU(6)$ quark model. The Δ deformation arises from the dressing of pion cloud, as represented in yellow area for E_{1+} . It corresponds to the principal value integral contribution in Eq. (5) and describes the off-energy-shell πN rescattering effects.

3.3 Extracted Properties of Higher Resonances

The meson-exchange πN model described in Sec. 2.1. has been extended to energies $W \leq 2$ GeV [15] and used to extract properties of higher resonances. We illustrate our scheme for S_{11} channel in the followings, where we include the ηN channel and enlarge the Hilbert space to accommodate as many resonances as would be required by the data. We assume that each contributing bare resonance R acquires a width by coupling to πN and ηN channels. Details can be found in [15].

The full t -matrix can be written as a system of coupled equations,

$$t_{ij}(E) = v_{ij}(E) + \sum_k v_{ik}(E) g_k(E) t_{kj}(E), \quad (10)$$

with i and j denoting the π and η channels and $E \equiv W$, the total c.m. energy. The potential v_{ij} is, as in Eq. (6), a sum of background (v_{ij}^B) and bare resonance (v_{ij}^R) terms, $v_{ij}(E) = v_{ij}^B(E) + v_{ij}^R(E)$, where $v_{\pi\pi}^B$ for the πN elastic channel is taken as obtained in Sec. 2.1. In channels involving η , the potential $v_{\eta\eta}^B$ is assumed to vanish because of the small ηNN coupling.

The bare resonance contribution arises from excitation and decay of the resonance R . The matrix elements of the potential $v_{ij}^R(E)$ can be symbolically expressed by

$$v_{ij}^R(q, q'; E) = \frac{f_i(\tilde{\Lambda}_i, q; E) g_i^{(0,R)} g_j^{(0,R)} f_j(\tilde{\Lambda}_j, q'; E)}{E - M_R^{(0)} + \frac{i}{2} \Gamma_R^{2\pi}(E)}, \quad (11)$$

where $M_R^{(0)}$ denotes the mass of bare resonance R ; q and q' are the pion (or eta) momenta in the initial and final states, and $g_{i/j}^{(0,R)}$ denotes the resonance vertex couplings. $\tilde{\Lambda}_i$ stands for a triple of cut-offs, $(\Lambda_N, \Lambda_R, \Lambda_\pi)$, defined in form factor $F_\alpha(p_\alpha^2) = \left[n\Lambda_\alpha^4 / (n\Lambda_\alpha^4 + (m_\alpha^2 - p_\alpha^2)^2) \right]^n$, with p_α the four-momentum and m_α the mass of particle α . In Eq. (11), we have included a phenomenological term $\Gamma_R^{2\pi}(E)$ in the resonance propagator to account for the $\pi\pi N$ decay channel. Therefore, our bare resonance propagator already contains a phenomenological “dressing” effect due to the coupling to $\pi\pi N$ channel. We use the parameterization of [30, 31] which has the correct threshold behavior and contains another cut-off. With this prescription we assume that any further non-resonant coupling to the $\pi\pi N$ channel can be neglected. All together, each resonance is generally described by 6 free parameters.

The generalization of the coupled-channel model to the case of N resonances with the same quantum numbers is then given by $v_{ij}^R(q, q'; E) = \sum_{n=1}^N v_{ij}^{R_n}(q, q'; E)$. The solutions of the coupled-channel equations of Eq. (10), with potentials given above were fitted to the πN phase shifts and inelasticity in all channels up to the F -waves and for $W \leq 2$ GeV. We obtain excellent description for both the real and the imaginary parts of the pion-nucleon scattering amplitudes in all cases except for the D_{35} and F_{17} channels. However, the fit to the data requires four additional resonances with very large widths, $S_{11}(1878)$, $D_{13}(2152)$, $P_{13}(2204)$, and $P_{31}(2100)$, which are not listed by the PDG [32].

The physical mass M_R , total width Γ_R , single-pion branching ratio $\beta_R^{1\pi}$, and background phase ϕ_R defined for each overlapping nucleon resonance R have been determined as explained in [15]. T -matrix poles have been calculated by three different techniques: analytic continuation into the complex energy plane, speed-plot, and regularization method [17]. Only the results for bare ($M_R^{(0)}$) and physical (M_R) resonance masses and total widths Γ_R are listed in the following Tables I and II and compared with listings of PDG, for the isospin- $\frac{3}{2}$ and isospin- $\frac{1}{2}$ resonances, respectively. More results can be found in [15]. One sees a qualitative agreement in general but considerable discrepancies in some cases, in particular for the widths of some higher resonances. Further investigations will be necessary to understand these differences in detail.

Table I. Bare ($M_R^{(0)}$) and physical (M_R) resonance masses and total widths Γ_R , all in units of MeV, for $I = 3/2$ resonances. Upper lines: our results, lower lines: PDG values [32].

N^*	$M_R^{(0)}$	M_R	Γ_R
$P_{33}(1232)$	1425	1233	132
***		1232 ± 1	118 ± 2
$P_{33}(1600)$	1575	1562	216
***		1600 ± 100	350 ± 100
$S_{31}(1620)$	1654	1616	160
***		1630 ± 30	142 ± 18
$D_{33}(1700)$	1690	1650	260
***		1710 ± 40	300 ± 100
$P_{31}(1750)$	1765	1746	554
*		1744 ± 36	300 ± 120
$S_{31}(1900)$	1796	1770	430
**		1900 ± 50	190 ± 50
$F_{35}(1905)$	1891	1854	534
***		1890 ± 25	335 ± 65
$P_{31}(1910)$	1953	1937	226
***		1895 ± 25	230 ± 40
$P_{33}(1920)$	1856	1827	834
***		1935 ± 35	220 ± 70
$D_{35}(1930)$	2100	2068	426
***		1960 ± 60	360 ± 140
$D_{33}(1940)$	2100	2092	310
*		2057 ± 110	460 ± 320
$F_{37}(1950)$	1974	1916	338
***		1932 ± 17	285 ± 50
$F_{35}(2000)$	2277	2260	356
**		2200 ± 125	400 ± 125
$P_{31}(xxx)$	2160	2100	492
$S_{31}(2150)$	2118	1942	416
*		2150 ± 100	200 ± 100

Table II. $I = 1/2$ resonances. Notations same as in Table I.

N^*	$M_R^{(0)}$	M_R	Γ
$P_{11}(1440)$	1612	1418	436
***		1445 ± 25	325 ± 125
$D_{13}(1520)$	1590	1520	94
***		1520 ± 5	115 ± 15
$S_{11}(1535)$	1559	1520	130
***		1535 ± 10	150 ± 25
$S_{11}(1650)$	1727	1678	200
***		1655 ± 10	165 ± 20
$D_{15}(1675)$	1710	1670	154
***		1675 ± 5	147 ± 17
$F_{15}(1680)$	1748	1687	156
***		1685 ± 5	130 ± 10
$D_{13}(1700)$	1753	1747	156
**		1700 ± 50	100 ± 50
$P_{11}(1710)$	1798	1803	508
**		1710 ± 30	180 ± 100
$P_{13}(1720)$	1725	1711	278
***		1725 ± 25	225 ± 75
$P_{13}(1900)$	1922	1861	1000
**		1879 ± 17	498 ± 78
$F_{15}(2000)$	1928	1926	58
**		1903 ± 87	490 ± 310
$D_{13}(2080)$	1972	1946	494
**		1804 ± 55	450 ± 185
$S_{11}(xxx)$	1803	1878	508
$S_{11}(2090)$	2090	2124	388
*		2180 ± 80	350 ± 100
$P_{11}(2100)$	2196	2247	1020
*		2125 ± 75	260 ± 100
$D_{13}(xxx)$	2162	2152	292
$P_{13}(xxx)$	2220	2204	406
$D_{15}(2200)$	2300	2286	532
**		2180 ± 80	400 ± 100

4. Summary

Some of the featured results of the Dubna-Mainz-Taipei (DMT) dynamical model for πN scattering and π^0 electromagnetic (EM) production are summarized. These include results for threshold production, deformation of $\Delta(1232)$, and the extracted properties, including masses and widths, of higher resonances below 2 GeV. The excellent agreement of DMT model's predictions with threshold π^0 production data, including the recent precision measurements from MAMI establishes results of the DMT model as a benchmark [33] for experimentalists and theorists in dealing with threshold pion production. In the first resonance region with low momentum transfer, DMT model provides an excellent description of the existing data and offers a dynamical picture for the $\Delta(1232)$ deformation. Namely, the bare Δ is almost spherical and the deformation of physical Δ arises from the dressing of the core by pion cloud.

Going beyond the first resonance region but below $W \leq 2$ GeV, the model was extended by in-

cluding the ηN channel and all the πN resonances with masses ≤ 2 GeV, up to the F waves. The effects of the $\pi\pi N$ channels are taken into account by introducing an effective width in the resonance propagators. The extended model gives an excellent fit to both πN phase shifts and inelasticity parameters in all channels up to the F waves and for energies below 2 GeV. However, the fit to the data requires four additional resonances with very large widths, $S_{11}(1878)$, $D_{13}(2152)$, $P_{13}(2204)$, and $P_{31}(2100)$, which are not listed by PDG [32]. In addition, the predicted values for the resonance masses and widths are compared to the listing of the PDG. In general, there is qualitative agreement but considerable discrepancies exist in some cases, in particular for the widths of some higher resonances. Further study will be necessary to understand these differences in detail.

Acknowledgement

Results summarized here have been obtained in collaborations with G.Y. Chen, D. Dreschel, C.T. Hung, S.S. Kamalov, C.C. Lee, T.-S.H. Lee, and L. Tiator. I dedicate this article to the memory of Mr. Chau-Chen Lee, the first author of Ref. [7], who recently passed away abruptly. I am indebted to L. Tiator for providing me with some of the figures shown.

References

- [1] H. Tanabe and K. Ohta, Phys. Rev. C **31** (1985) 1876.
- [2] S. N. Yang, J. Phys. G **11** (1985) L205.
- [3] H. Kamano, S. X. Nakamura, T.-S. H. Lee, and T. Sato, Phys. Rev. C **88** (2013) 035209.
- [4] H. Kamano, talk in this meeting.
- [5] E. Mazzucato et al., Phys. Rev. Lett. **57**, 3144 (1986); R. Beck *et al.*, *ibid.* **65** (1990) 1841.
- [6] S. N. Yang, Phys. Rev. C **40** (1989) 1810.
- [7] C.C. Lee, S.N. Yang, and T.-S.H. Lee, J. Phys. G **17** (1991) L131.
- [8] C. T. Hung, S. N. Yang, and T.-S. H. Lee, J. Phys. G **20** (1994) 1531.
- [9] C. T. Hung, S. N. Yang, and T.-S. H. Lee, Phys. Rev. C **64** (2001) 034309.
- [10] S.S. Kamalov and S. N. Yang, Phys. Rev. Lett. **83** (1999) 4494.
- [11] S.S. Kamalov *et al.*, Phys. Rev. C **64** (2001) 032201(R).
- [12] S. S. Kamalov *et al.*, Phys. Lett. B **522** (2001) 27.
- [13] E. D. Cooper and B. K. Jennings, Nucl. Phys. A **483** (1988) 601.
- [14] G. Y. Chen *et al.*, Nucl. Phys. A **723** (2003) 447.
- [15] G. Y. Chen *et al.*, Phys. Rev. C **76** (2007) 035206.
- [16] V. Pascalutsa, M. Vanderhaeghen, and S. N. Yang, Phys. Repts. **437** (2007) 125.
- [17] L. Tiator *et al.*, Phys. Rev. C **82** (2010) 055203.
- [18] M. G. Olsson and E. T. Osypowsky, Nucl. Phys. B **87** (1975) 399.
- [19] Proc. 7th Int'l Workshop on Chiral Dynamics (CD12), PoS CD12 (2012) and references contained therein.
- [20] M. Hilt, S. Scherer, and L. Tiator, Phys. Rev. C **87** (2013) 045204, and references contained therein.
- [21] S. Scherer, talk in this meeting.
- [22] V. Bernard, N. Kaiser, and Ulf-G. Meißner, Phys. Lett. B **383** (1996) 116, and references contained therein.
- [23] M. Weis *et al.* [A1 Collaboration at MAMI] Eur. Phys. J. A **38**, (2008) 27.
- [24] S. Schumann *et al.* [A2 Collaboration at MAMI], Phys. Lett. B **750**, (2015) 252.
- [25] O. Hanstein, D. Drechsel, and L. Tiator, Nucl. Phys. A. **632**, (1998) 561.
- [26] R. A. Arndt, I. I. Strakovsky and R. L. Workman, Phys. Rev. C **53**, (1996) 430.
- [27] R. Beck *et al.* Phys. Rev. Lett. **78**, (1997) 606; G. Blanpied *et al.* Phys. Rev. Lett. **79**, (1997) 4337.
- [28] S. S. Hsiao, C. T. Hung, J. L. Tsai, S. N. Yang, and Y. B. Dong, Few-Body Systems **25**, (1998) 55.
- [29] L. Tiator *et al.*, Eur. Phys. J. **17**, (2003) 357.
- [30] A. I. L'vov, V. A. Petrun'kin, and M. Schumacher, Phys. Rev. C **55**, (1997) 359.
- [31] D. Drechsel, O. Hanstein, S.S. Kamalov, and L. Tiator, Nucl. Phys. A **645**, (1999) 145.
- [32] W.-M. Yao et al. (Particle Data Group), J. Phys. G **33**, (2014) 1.
- [33] DMT model can be accessed on-line via <http://portal.kph.uni-mainz.de/MAID//dmt/dmt2001.html>